ACSNANO

www.acsnano.org

ARTICLE

Mucoadhesive and Self-Assembled Chitosan Oligosaccharide-Glycyrrhizin Nanoparticle for Oral Nanotherapeutic in Inflammatory Bowel Disease

Gayoung Lim,[#] Ha Rin Kim,[#] Chaerim Yoo,[#] Yu Kyung Oh, Yeon Soo Park, Sijin Park, Seonmi Jang, Lia Priscilla, and Dong Yun Lee*

Cite This: https://doi.org/10.1021/acsnano.5c09985

Read Online

ACCESS | Metrics & More | Article Recommendations | Supporting Information

ABSTRACT: **Inflammatory bowel disease (IBD) is a chronic inflammatory disorder characterized by severe oxidative stress and intestinal barrier dysfunction. Conventional oral therapies are often limited by low bioavailability and off-target effects. Herein, we report the development of mucoadhesive nanotherapeutics engineered from low molecular weight chitosan oligosaccharide (COS) and glycyrrhizin (GL), a natural anti-inflammatory compound. Hydrophilic COS, selected for its potent antioxidant and mucoadhesive properties, was chemically conjugated with hydrophobic GL to facilitate self-assembly into stable COS-GL nanoparticles (~129 nm). These nanoparticles exhibit enhanced retention at inflamed intestinal sites and preferential uptake by activated immune and epithelial cells. In vitro evaluations using transwell coculture systems and intestinal organoids revealed that COS-GL nanoparticles effectively suppress pro-inflammatory cytokine secretion, promote M1-to-M2 macrophage remodeling, neutralize reactive oxygen species (ROS), and restore intestinal barrier integrity by upregulating tight junction proteins. In a DSS-induced colitis mouse model, orally administered COS-GL nanoparticles outperform both their individual components and the standard therapeutic 5-aminosalicylic acid (5-ASA), mitigating inflammation and promoting mucosal healing. These findings establish COS-GL nanoparticles as a promising and effective nanotherapeutic platform for the targeted oral treatment of IBD.**

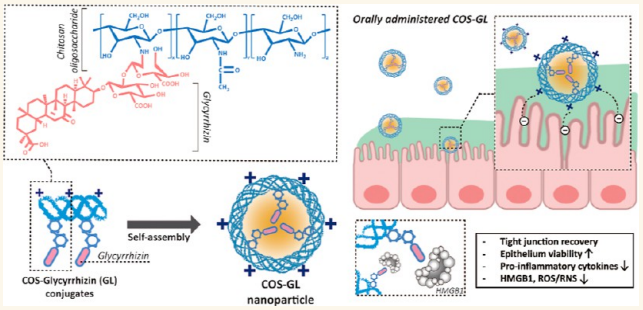

KEYWORDS: *inflammatory bowel disease, chitosan oligosaccharide, glycyrrhizin, mucoadhesive nanoparticles, intestinal barrier restoration, immune modulation, intestinal organoids*

Inflammatory bowel disease (IBD), which includes ulcerative colitis (UC) and Crohn's disease (CD), is a chronic, relapsing inflammatory disorder of the gastrointestinal (GI) tract that imposes a significant clinical and economic burden worldwide.[1−3] The complex pathophysiology of IBD involves a dysfunctional intestinal barrier, dysregulated immune activation, and persistent production of damage-associated molecular patterns (DAMPs) and reactive oxygen species (ROS), which collectively fuel chronic inflammation and tissue damage.[4−6] Specifically, the disruption of critical tight junction proteins such as occludin and Zonula Occludens-1 (ZO-1) compromises intestinal barrier integrity, leading to increased permeability, microbial translocation, and an exacerbated, self-perpetuating inflammatory response.[7−9]

Current therapeutic strategies for IBD, including 5-aminosalicylic acid (5-ASA), corticosteroids, and biologics like anti-TNF-α antibodies, primarily aim to suppress inflammation.[10,11] However, their efficacy is often constrained by systemic side effects, poor bioavailability, high treatment costs, and the development of drug resistance.[12] The absence of targeted delivery to inflamed intestinal tissues results in suboptimal therapeutic outcomes and significant off-target toxicity.[13−15]

Received: June 14, 2025
Revised: August 13, 2025
Accepted: August 13, 2025

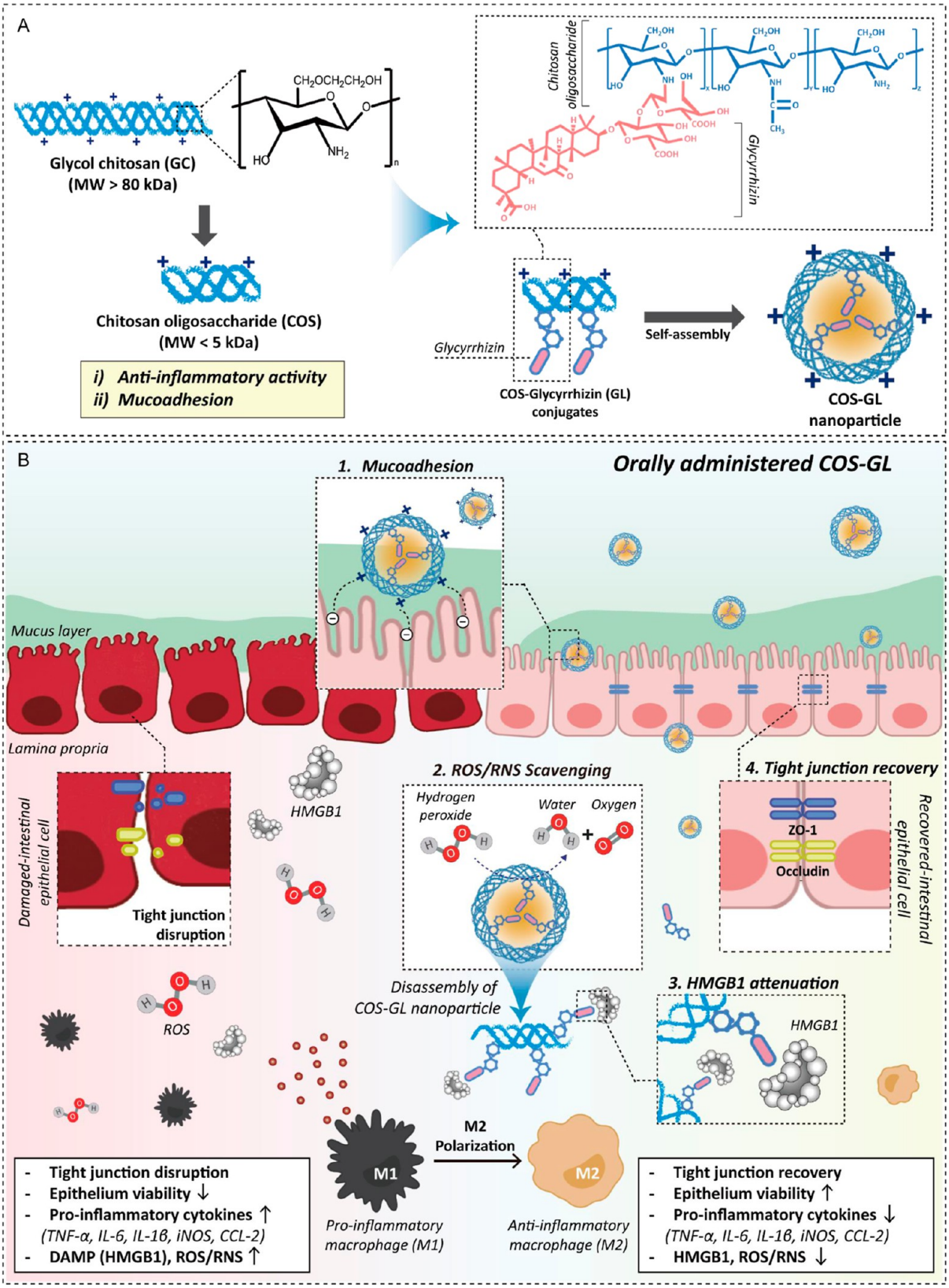

Figure 1. Schematic illustration of COS-GL nanoparticles, incorporating enhanced mucoadhesion and HMGB1 attenuation for targeted therapy in the colitis microenvironment. (A) Schematic diagram of the synthesis route of COS-GL. (B) Schematic diagram depicting the role of COS-GL nanoparticles. Following oral administration, the nanoparticles adhere to the intestinal mucus layer, scavenge ROS and RNS, attenuate HMGB1-mediated inflammatory signaling, and restore tight junction proteins. These effects collectively suppress pro-inflammatory cytokines, promote M2 macrophage polarization, and enhance intestinal barrier integrity.

https://doi.org/10.1021/acsnano.5c09985
ACS Nano XXXX, XXX, XXX−XXX

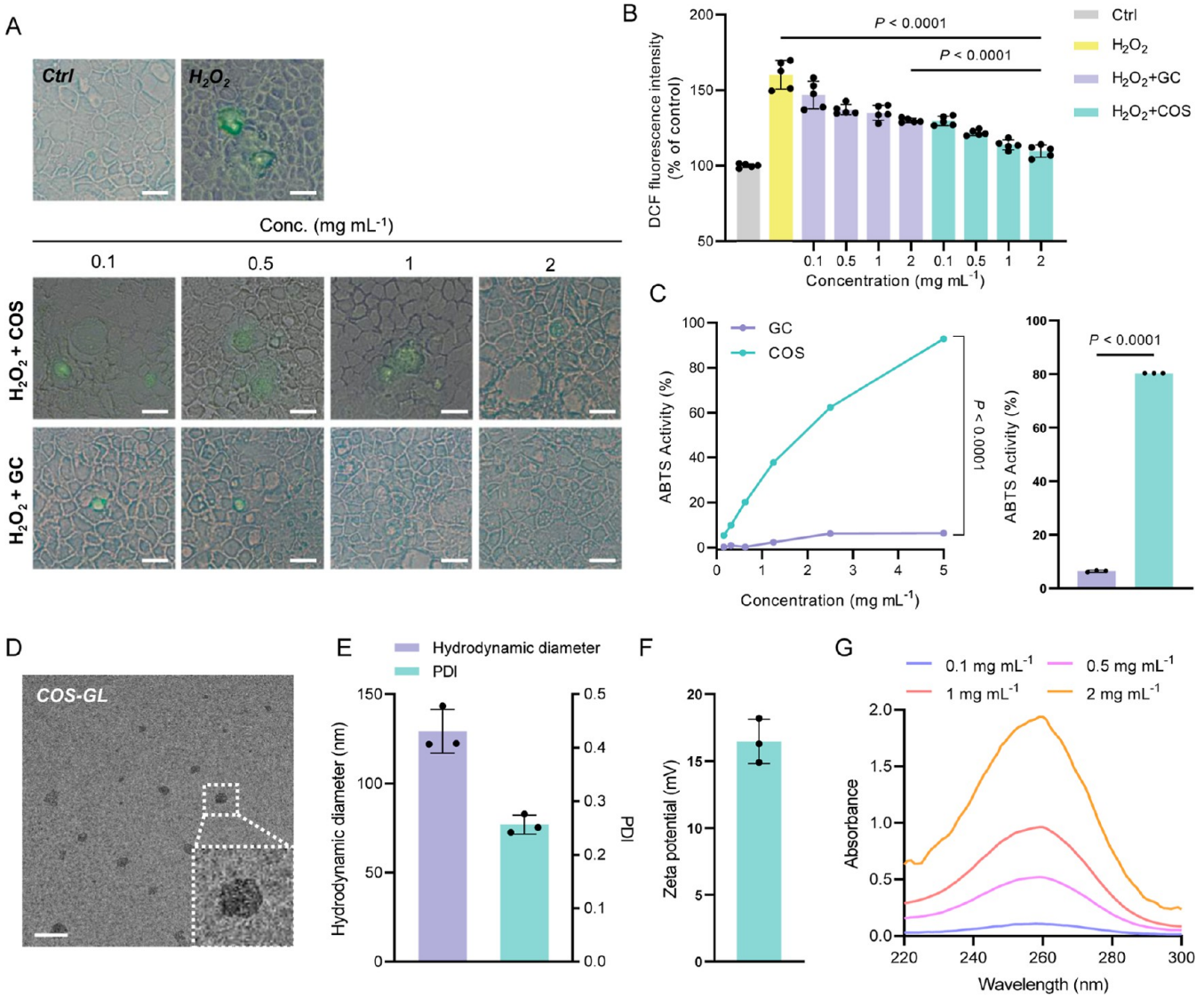

Figure 2. Comparative analysis between chitosan oligosaccharide (COS) and glycol chitosan (GC) and characterization of COS-GL nanoparticles. (A) Fluorescence microscopic images of DCF-DA stained Caco-2 cells treated with GC and COS. Scale bar: 50 μm. (B) Quantitative analysis of DCF-DA assay of Caco-2 cells incubated with GC and COS at various concentrations, respectively. Data are expressed as mean ± SD (n = 5). (C) ABTS radical scavenging activity (%) using GC and COS at various concentrations and equivalent amounts of amine groups. (D) TEM image of COS-GL nanoparticles, showing their spherical morphology. Scale bar: 0.2 μm. (E) Hydrodynamic size and PDI of COS-GL nanoparticles measured by DLS. Data are expressed as mean ± SD (n = 3). (F) Zeta potential (mV) of COS-GL nanoparticles, indicating surface charge. Data are expressed as mean ± SD (n = 3). (G) UV−vis absorption spectra of COS-GL nanoparticles at various concentrations. Absorption spectra of COS-GL nanoparticles at 0.1, 0.5, 1, and 2 mg·mL^{-1}, displaying the same characteristic peak, indicating successful incorporation of GL into the nanoparticles. Statistical significance was determined by unpaired, two-tailed t-test in (B).

Consequently, there is a critical unmet need for innovative therapeutic platforms that can enhance drug localization, prolong retention at inflamed sites, and minimize systemic exposure. One promising strategy involves targeting high-mobility group box 1 (HMGB1), a DAMP that is highly expressed in the intestinal tissues of IBD patients. HMGB1 plays a pivotal role in amplifying inflammatory pathways via the Receptor for advanced glycation endproducts (RAGE) and toll-like Rrceptors (TLRs).[16−19] This signaling cascade fosters an inflammatory microenvironment (IME) rich in ROS, which perpetuates chronic inflammation.[20,21] Therefore, therapeutic modalities that inhibit HMGB1 activity and ameliorate the IME are promising alternatives for IBD management.

Glycyrrhizin (GL), a natural triterpenoid from licorice root, is a known HMGB1 inhibitor with potent anti-inflammatory and antioxidant properties.[22−24] However, its clinical utility is severely hampered by poor water solubility, low oral bioavailability, and rapid clearance from the GI tract.[25] To overcome these limitations, nanomedicine offers a compelling approach. Here, we developed mucoadhesive nanoparticles by conjugating GL to chitosan oligosaccharide (COS) (Figure 1A). Compared to high-molecular-weight chitosan like glycol chitosan (GC),[26,27] COS possesses superior aqueous solubility, intrinsic bioactivity, and enhanced antioxidative and mucoadhesive properties.[28,29] Its smaller molecular size may facilitate deeper penetration into inflamed tissues, while its inherent bioactivity has been shown to enhance tight junction protein

https://doi.org/10.1021/acsnano.5c09985
ACS Nano XXXX, XXX, XXX−XXX

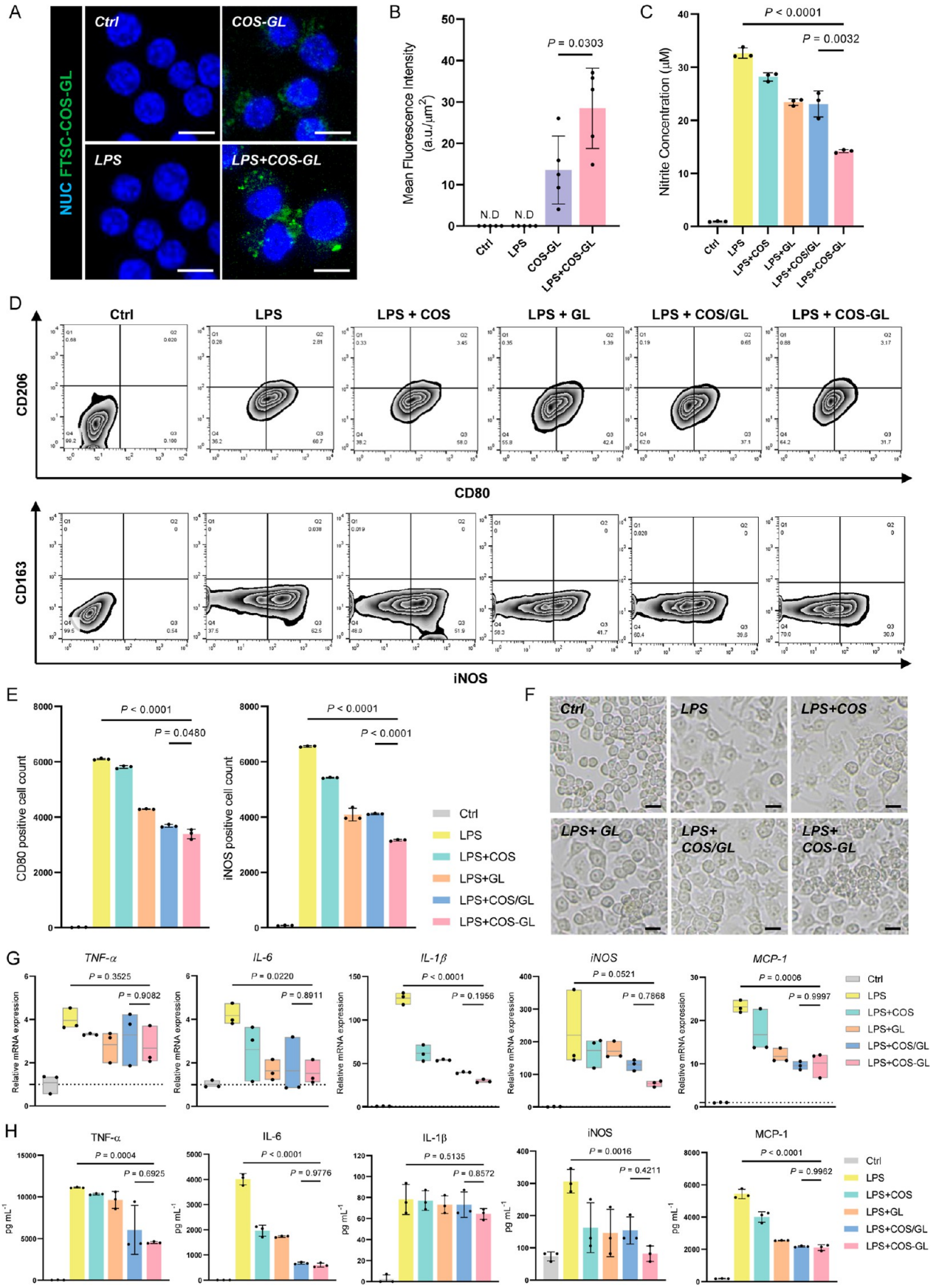

Figure 3. Anti-inflammatory activity of COS-GL nanoparticles. (A) Representative confocal microscopy images showing the uptake of FTSC-labeled COS-GL in LPS-activated and untreated RAW 264.7 macrophages. Nuclei were counterstained with DAPI. Scale bar: 10 μm. (B) Mean fluorescence intensity of FTSC-labeled COS-GL. Quantification of mean fluorescence intensity of FTSC (green) using ImageJ

https://doi.org/10.1021/acsnano.5c09985
ACS Nano XXXX, XXX, XXX−XXX

Figure 3. continued

software. Data are expressed as mean ± SD (n = 5). (C) Reactive nitrogen species (RNS) inhibition effect of COS, GL, COS/GL, and COS-GL in LPS treated RAW 264.7 cells. Data are expressed as mean ± SD (n = 3). (D) Effects of COS, GL, COS/GL, and COS-GL on M1 and M2 polarization in RAW 264.7 cells stimulated with LPS by measuring the expression of cell surface markers with flow cytometry. M1 cell surface markers included CD80 and iNOS; M2 cell surface markers included CD206 and CD163. Filled histograms represent iso-type-matched control antibody staining. (E) Graph of M1 (CD80, iNOS positive) cell counts indicates mean fluorescence intensity of stained cells. Data are expressed as mean ± SD (n = 3). (F) Morphological changes of LPS-stimulated RAW 264.7 cells after treatment with COS, GL, COS/GL, and COS-GL. Scale bar: 20 μm. (G) qRT-PCR results of proinflammatory cytokines (TNF-α, IL-6, IL-1β, iNOS, and MCP-1). Data are expressed as mean ± SD (n = 3). (H) Investigation of pro-inflammatory cytokines (TNF-α, IL-6, IL-1β, iNOS, and MCP-1) by ELISA. Data are expressed as mean ± SD (n = 3). Statistical significance was determined by unpaired, two-tailed t-test in (B,C), (E,G), and (H).

expression, directly contributing to intestinal barrier repair.[30−32] In this study, we engineered and characterized mucoadhesive chitosan oligosaccharide-glycyrrhizin (COS-GL) nanoparticles as an advanced oral nanomedicine for IBD therapy (Figure 1B). We systematically evaluated their therapeutic efficacy using in vitro models, including transwell cocultures and intestinal organoids, and an in vivo dextran sulfate sodium (DSS)-induced colitis mouse model. Our findings demonstrate that COS-GL nanoparticles effectively target inflamed intestinal tissues, mitigate oxidative stress, modulate immune responses, and restore intestinal barrier function, establishing their potential as a next-generation therapeutic for IBD.

RESULTS AND DISCUSSION

Comparative Analysis of Antioxidative and Mucoadhesive Properties: Chitosan Oligosaccharide (COS) vs Glycol Chitosan (GC). For the development of nano-therapeutic platform, we first compared the intrinsic therapeutic properties of low-molecular -weight chitosan oligosaccharide (COS, <5 kDa) over the more conventional glycol chitosan (GC, ∼250 kDa).[33] The rationale for this choice is that the lower molecular weight of COS affords greater chain flexibility and a higher density of available amine groups, which enhances water solubility, mucosal diffusion, and intrinsic antioxidant properties,[34,35] making it an ideal candidate for treating IBD.

To experimentally validate this selection, we directly compared the intrinsic therapeutic properties of COS and GC. In an ABTS radical scavenging assay, COS exhibited vastly superior activity, reducing ROS by 80.3% compared to only 6.4% for GC. This enhanced efficacy was confirmed in a cell-based DCFH-DA assay, where COS treatment of Caco-2 cells resulted in a 50.5% reduction in intracellular ROS, significantly outperforming the 30.2% reduction by GC (Figure 2A−C). These results are consistent with reports that lower molecular weight chitosan derivatives possess greater antioxidant capacity, likely due to their increased solubility and reactivity. Next, we assessed mucoadhesion, a critical property for its oral IBD therapeutics, as it ensures prolonged retention at inflamed sites. In a turbidity assay with porcine mucin, COS again demonstrated superior performance, inducing a significant change in absorbance (ΔA_{500} = 0.06) compared to GC (ΔA_{500} = 0.02). This indicates stronger electrostatic interactions with negatively charged mucin glycoproteins, which is crucial for prolonging retention at inflamed intestinal sites (Figure S1).[36]

Given its decisively superior performance in both antioxidative and mucoadhesive properties, COS was confirmed as the optimal polymeric scaffold for our nanoparticle design. These results support the application of COS as a unique and functionally superior material for developing effective IBD therapeutics.

Physicochemical Characterization of Self-Assembled COS-GL Nanoparticles. To prepare self-assembled COS-GL nanoparticles, the hydrophilic COS polysaccharide was chemically conjugated with hydrophobic GL molecules. To this end, GL itself was oxidized to generate the aldehyde group via the ring opening of glucuronic acid. Then, COS-GL nanoparticles were synthesized via a Schiff base reaction between the oxidized glycyrrhizin (oGL) and COS, followed by reductive stabilization (Figure S2).[37] FT-IR spectroscopy confirmed successful conjugation, evidenced by the disappearance of characteristic primary amine and aldehyde peaks and the retention of key functional groups from the parent molecules (Figure S3). ^{1}H NMR analysis further validated the conjugation, showing peaks corresponding to COS glucosamine units and GL-specific groups, with the disappearance of the aldehyde proton signal confirming the reaction (Figure S4).

Transmission electron microscopy (TEM) revealed that the nanoparticles were uniform and spherical, with a core diameter of 67.48 ± 10.16 nm (Figures 2D and S5), an ideal size for tissue penetration and cellular uptake in the inflamed gut.[38,39] A low critical micelle concentration (CMC) of 0.1012 mg·mL^{-1}, determined by a pyrene fluorescence assay, indicated high thermodynamic stability in dilute aqueous solutions (Figure S6). Dynamic light scattering (DLS) analysis confirmed a hydrodynamic size of 129.27 ± 12.24 nm and a low polydispersity index (PDI) of 0.256, reflecting their uniform size distribution in solution (Figure 2E). The nanoparticles exhibited a positive zeta potential of +16.47 ± 1.66 mV (Figure 2F), which is advantageous for promoting electrostatic interactions with the negatively charged intestinal mucosa, thereby enhancing mucoadhesion.[40] UV−vis spectroscopy confirmed an efficient GL loading of approximately 80% (w/w) (Figures 2G, S7 and Table S1). Collectively, these data confirm the successful synthesis of well-defined, stable COS-GL nanoparticles with physicochemical properties ideally suited for oral IBD therapy.

COS-GL Nanoparticles Exhibit Potent Anti-Inflammatory Activity In Vitro. Based on cytotoxicity assays in RAW 264.7 macrophages and Caco-2 epithelial cells, a nontoxic concentration of 1 mg·mL^{-1} was used for all functional experiments (Figure S8). Fluorescence microscopy revealed that FITC-labeled COS-GL nanoparticles were preferentially internalized by lipopolysaccharide (LPS)-activated macrophages and H_2O_2-stressed Caco-2 cells compared to their nonstimulated counterparts, indicating targeted uptake at inflamed sites (Figures 3A,B, and S9). In LPS-stimulated macrophages, COS-GL treatment significantly inhibited nitric

https://doi.org/10.1021/acsnano.5c09985
ACS Nano XXXX, XXX, XXX−XXX

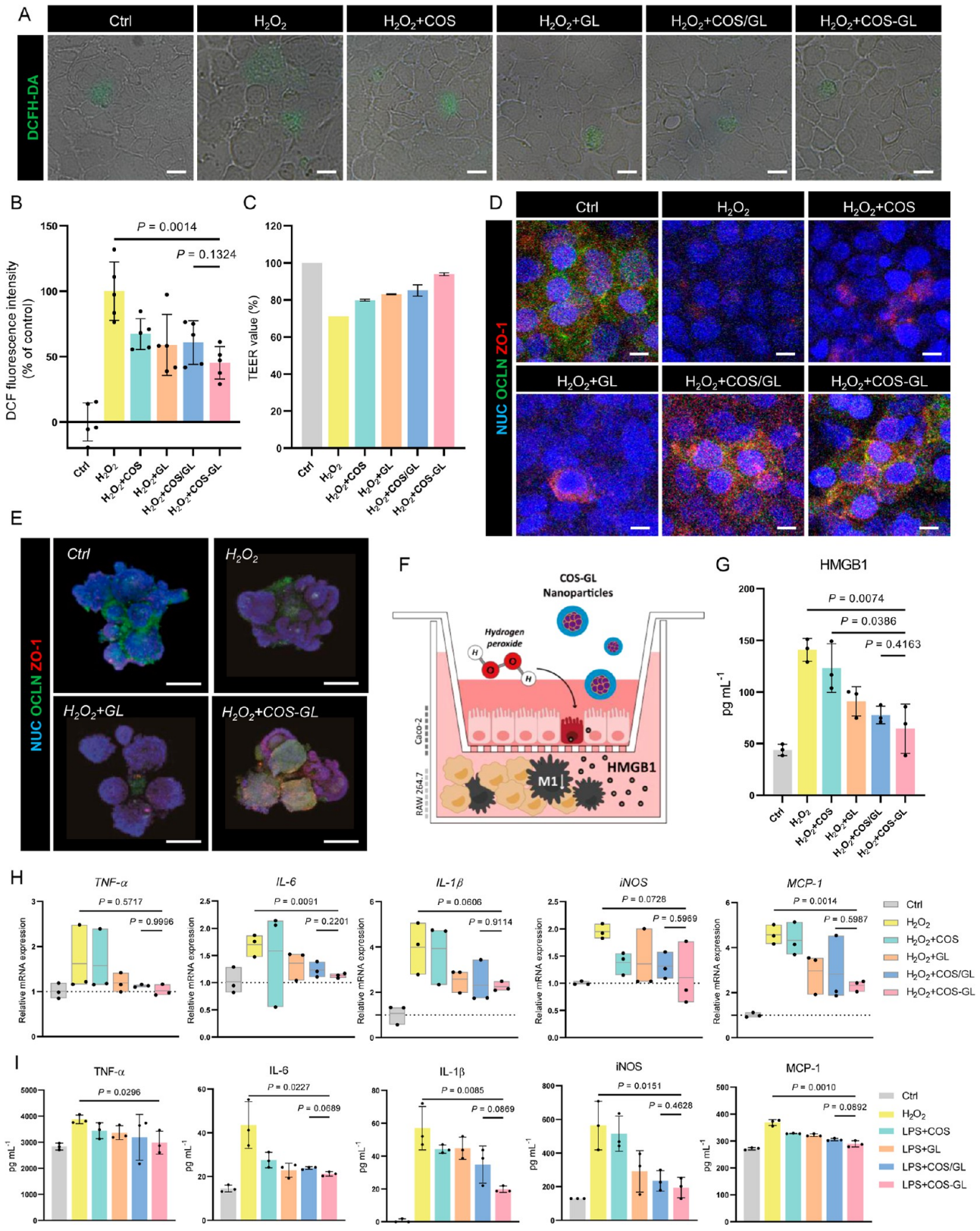

Figure 4. Antioxidant effect and restoration of intestinal barrier function of COS-GL. (A,B) Fluorescence microscopic images (A) and quantitative analysis (B) of DCF-DA stained Caco-2 cells treated with COS, GL, COS/GL, and COS-GL, respectively. Data are expressed as mean ± SD (n = 5). Scale bar: 20 μm. (C) TEER values of H_2O_2-stimulated Caco-2 cells treated with COS, GL, COS/GL, and COS-GL, showing restoration of barrier function. Data are expressed as mean ± SD (n = 2). (D) Fluorescence images of Caco-2 cell monolayers costained with occludin (green), ZO-1 (red), and nuclei (DAPI, blue), showing tight junction protein expression and structural integrity after treatment with COS, GL, COS/GL, and COS-GL under oxidative stress (+H_2O_2) conditions. Scale bar: 50 μm. (E) Fluorescence images of H_2O_2-stimulated intestinal organoids treated with GL or COS-GL, costained with occludin (green), ZO-1 (red), and nuclei (DAPI, blue). Scale bar: 100 μm. (F) Schematic illustration of the transwell system mimicking the normal intestinal microenvironment. Caco-2 cells

https://doi.org/10.1021/acsnano.5c09985
ACS Nano XXXX, XXX, XXX−XXX

Figure 4. continued

were cultured in the apical chamber to form a monolayer, and RAW 264.7 macrophages were seeded in the basal chamber. (G) Protein levels of HMGB1 in the basal chamber supernatant, measured by ELISA. Data are expressed as mean ± SD (n = 3). (H) qRT-PCR results of proinflammatory cytokines (TNF-α, IL-6, IL-1β, iNOS, and MCP-1) in the basal chamber supernatant. Data are expressed as mean ± SD (n = 3). (I) Investigation of pro-inflammatory cytokines (TNF-α, IL-6, IL-1β, iNOS, and MCP-1) in the basal chamber supernatant by ELISA. Data are expressed as mean ± SD (n = 3). Statistical significance was determined by unpaired, two-tailed t-test in (B,G), (H,I).

oxide (NO) production by 2.3-fold relative to the LPS control, an effect markedly greater than that of the individual components or their physical mixture (Figure 3C). This highlights the enhanced bioavailability and synergistic activity afforded by the nanoparticle formulation.

Flow cytometry analysis demonstrated that COS-GL nanoparticles potently suppressed M1 polarization ($CD80^+$/$iNOS^+$ cells) in LPS-stimulated macrophages, outperforming all control treatments (Figure 3D,E).[41] This anti-inflammatory effect was further confirmed by the reversal of M1-polarized macrophage morphology (Figure 3F). Consistent with these findings, COS-GL treatment significantly downregulated the expression and secretion of key pro-inflammatory cytokines, including TNF-α (59.3% reduction), IL-6 (85.1% reduction), IL-1β (17.8% reduction), MCP-1 (61.3% reduction), and iNOS (73.3% reduction) at both the mRNA and protein levels (Figure 3G,H). The superior immunomodulatory activity of COS-GL underscores the therapeutic benefit of targeted cellular uptake and localized drug action.

Antioxidant Activity of COS-GL Nanoparticles in Restoring Intestinal Barrier Function. In H_2O_2-stressed Caco-2 cells, COS-GL nanoparticles markedly reduced intracellular ROS levels, exhibiting superior scavenging ability compared to COS, GL, or their physical mixture, which is attributable to the synergistic antioxidant action within the nanoparticle structure (Figure 4A,B).[42] Oxidative stress-induced barrier disruption was assessed in Caco-2 monolayers by measuring transepithelial electrical resistance (TEER). Exposure to H_2O_2 caused a sharp drop in TEER, indicating compromised tight-junction integrity. Treatment with COS-GL nanoparticles prompted a significant recovery, restoring TEER values to near-control levels and demonstrating superior performance over all control groups (Figures 4C and S10). Immunofluorescence imaging corroborated these functional data, revealing that COS-GL treatment restored the continuous, cortical localization of the tight junction proteins occludin and ZO-1, which were severely disrupted by H_2O_2 (Figure 4D). These findings were validated in a more physiologically relevant murine intestinal organoid model. H_2O_2-induced oxidative stress disrupted occludin and ZO-1 expression in vehicle-treated organoids (Figure 4E).[43] While GL alone offered partial protection, COS-GL treatment demonstrated superior efficacy, restoring the expression of both tight junction proteins to levels comparable to the healthy control group, with a 3.2-fold and 2.7-fold increase in occludin and ZO-1 expression, respectively (Figure S11).

To simulate the IBD microenvironment, we used a transwell coculture system with Caco-2 epithelial cells and RAW 264.7 macrophages (Figure 4F). H_2O_2-induced damage to the Caco-2 monolayer led to the release of HMGB1, which subsequently activated the underlying macrophages.[44] Treatment with COS-GL nanoparticles significantly suppressed the production of pro-inflammatory cytokines (TNF-α, IL-6, IL-1β, MCP-1) and key inflammatory mediators (iNOS, HMGB1) in the macrophages, demonstrating greater efficacy than all control treatments (Figures 4G–I and S12). This highlights the nanoparticle's ability to disrupt the inflammatory feedback loop between epithelial and immune cells. These findings collectively underscore the multifaceted therapeutic activity of COS-GL nanoparticles, which simultaneously neutralize ROS, interrupt downstream inflammatory signaling, and restore epithelial barrier integrity.

Therapeutic Efficacy of COS-GL Nanoparticles in a DSS-Induced Colitis Mouse Model. The in vivo therapeutic potential of the COS-GL nanoparticles was evaluated in a well-established dextran sulfate sodium (DSS)-induced acute colitis model in C57BL/6 mice. To ensure clinical relevance and reproducibility, treatment efficacy was assessed using standard end points, including the disease activity index (DAI), colon length, and detailed histopathological analysis.[45,46] As depicted in the experimental design (Figure 5A), mice in the vehicle-treated group exhibited severe colitis symptoms, including a drastic body loss of approximately 28% and a 50% mortality rate by the end of the study. In contrast, daily oral administration of COS-GL nanoparticles (50 $mg{\cdot}kg^{-1}$) led to a robust recovery of body weight, significantly outperforming the individual components (COS and GL) and the clinical standard 5-ASA (50 $mg{\cdot}kg^{-1}$) (Figure 5B). This superior efficacy was further confirmed by the disease activity index (DAI), a composite score reflecting weight loss, stool consistency, and rectal bleeding. The COS-GL treatment group displayed the lowest disease activity index (DAI) scores throughout the experiment and, critically, maintained a 100% survival rate, highlighting its life-sustaining potential (Figure 5C,D). The enhanced performance of COS-GL nanoparticles, particularly when compared to 5-ASA, which is known for its limited efficacy in severe colitis due to low colonic bioavailability and rapid systemic clearance,[47,48] can be attributed to the nanoparticle's mucoadhesive properties, which promote prolonged intestinal retention and sustained, localized anti-inflammatory action.

Macroscopic examination provided further evidence of therapeutic efficacy. DSS treatment induced significant colon shortening—a hallmark of severe inflammation—which was effectively prevented by COS-GL treatment. The colon length in the COS-GL group (5.45 cm) was nearly restored to that of the healthy control group (6.3 cm) and was significantly longer than in all other treatment groups (Figure 5E,F). Furthermore, splenomegaly, an indicator of systemic inflammation, was markedly attenuated in the COS-GL-treated group, suggesting a reduction in the systemic immune response (Figure S13). Finally, we assessed the systemic safety of the nanoformulation. Histopathological analysis of major organs, including the liver, kidneys, spleen, lungs, and heart, revealed no signs of inflammation, necrosis, or structural damage in any of the treatment groups (Figure S14). This was corroborated by blood biochemistry tests performed on day 14, which showed no significant abnormalities in hepatic or renal parameters, confirming the excellent systemic safety and biocompatibility

https://doi.org/10.1021/acsnano.5c09985
ACS Nano XXXX, XXX, XXX−XXX

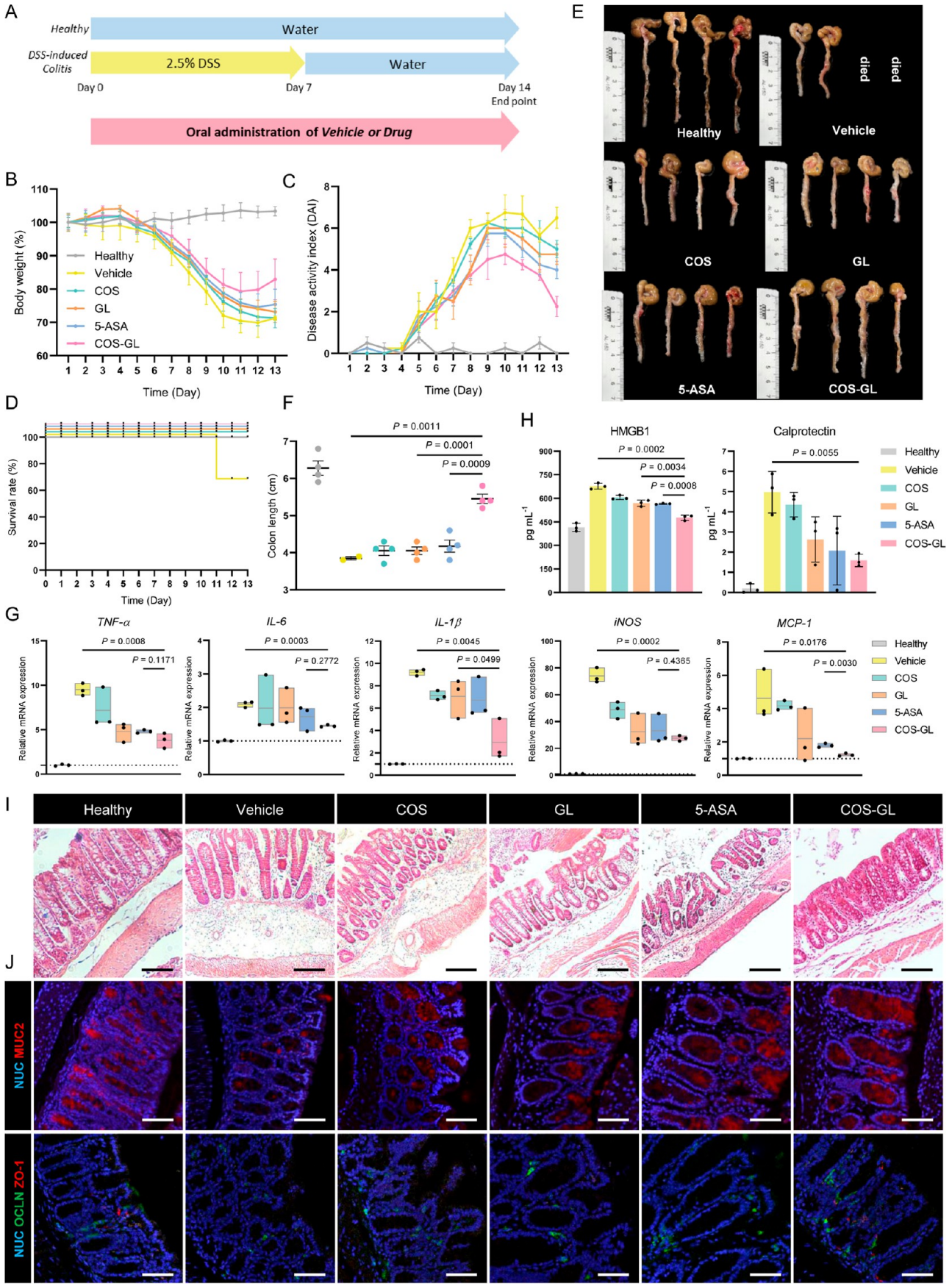

Figure 5. Therapeutic efficacy of COS-GL nanoparticles in DSS-Induced colitis mouse model. (A) Experimental design for DSS-induced colitis, including dosing schedule and treatment groups (healthy, vehicle, COS, GL, 5-ASA, and COS-GL). DSS was administered in drinking water (2.5%) for 7 days, followed by water. Treatments included vehicle or oral doses of 10 mg·kg^{-1} COS, 40 mg·kg^{-1} GL, 50 mg·kg^{-1} 5-

https://doi.org/10.1021/acsnano.5c09985
ACS Nano XXXX, XXX, XXX−XXX

Figure 5. continued

ASA, or 50 mg·kg^{-1} COS-GL nanoparticles. (B) Daily body weight changes (%) of mice over 13 days. Data are expressed as mean ± SD (n = 4 biological independent animals). (C) DAI scores were monitored daily. Data are expressed as mean ± SD (n = 4 biological independent animals). (D) Survival rate (%) for each group. Data are expressed as mean ± SD (n = 4 biological independent animals). (E) Images of the colon in each group on day 14. (F) Colon length in each group measured on day 14. Data are expressed as mean ± SD (n = 4 biological independent animals). (G) Relative mRNA expression levels of pro-inflammatory cytokines (TNF-α, IL-6, MCP-1, IL-1β, and iNOS) in colonic tissues of DSS-induced colitis mice. Data are normalized to GAPDH expression. Data are expressed as mean ± SD (n = 3). (H) Protein expression levels of inflammation-related markers (HMGB1 and calprotectin) in colonic tissues of DSS-induced colitis mice. Data are expressed as mean ± SD (n = 3). (I) Hematoxylin and eosin (H&E) staining of colonic sections from mice on day 14, illustrating epithelial damage and immune cell infiltration. Scale bar: 200 μm. (J) Immunohistochemical staining of colonic tissues. Upper panel; MUC2 (red) and nuclei (DAPI, blue) indicating mucin production and restoration of the mucus layer. Scale bar: 200 μm. Bottom panel; Occludin (green), ZO-1 (red), and nuclei (DAPI, blue), showing tight junction protein expression and restoration of intestinal barrier integrity. Scale bar: 200 μm. Statistical significance was determined by unpaired, two-tailed t-test in (F,G,H).

of the orally administered COS-GL nanoparticles (Figure S15).

Remodeling the Inflammatory Microenvironment and Promoting Barrier Repair. To elucidate the mechanisms underlying the therapeutic efficacy of COS-GL nanoparticles, we performed detailed molecular and histological analyses on colonic tissues. Quantitative RT-PCR analysis revealed that COS-GL treatment significantly downregulated the mRNA expression of key pro-inflammatory cytokines, including *Tnf-α*, *Il-6*, *Il-1β*, *Mcp-1*, and *iNos*, compared to the vehicle group (Figure 5G). Notably, COS-GL exhibited the most profound cytokine suppression, surpassing the effects of the clinical standard 5-ASA. Furthermore, COS-GL treatment restored the expression of the DAMP molecule HMGB1 and the clinical biomarker fecal calprotectin (CALP) to levels comparable to the healthy control, outperforming all other groups (Figure 5H). Mechanistically, glycyrrhizin (GL) is known to inhibit HMGB1 by inserting its triterpene core and glucuronic acid epitope into a key binding pocket of the HMGB1 domain.[49] In our synthesis, only the aldehyde group of oxidized GL (oGL) is consumed during Schiff base formation, leaving this critical pharmacophore structurally intact and functionally available. The potent inhibition of HMGB1 observed in vivo confirms that the drug moiety remains active postconjugation. Moreover, the superior HMGB1 suppression by COS-GL compared to free GL suggests a synergistic benefit derived from the nanoformulation, which enhances localized delivery and cellular uptake.

Histological analysis of H&E-stained colonic sections corroborated these molecular findings. COS-GL treatment effectively preserved intestinal architecture, preventing the massive immune cell infiltration and goblet cell depletion seen in the vehicle group (Figure 5I). This mucosal healing was further confirmed by immunohistochemical staining, which showed that COS-GL treatment significantly restored the protective mucus layer, evidenced by increased MUC2 expression (Figure 5J). Finally, COS-GL treatment effectively re-established the expression and proper localization of the tight junction proteins occludin and ZO-1 at epithelial junctions, thereby reinforcing the intestinal barrier to prevent the translocation of luminal antigens that perpetuate inflammation.[8,50] This multifaceted healing effect was visibly more pronounced than that observed with 5-ASA, underscoring the superiority of the COS-GL nanoparticle formulation. While a microbiome analysis was not performed in this study, it is worth noting that COS has been shown to promote the growth of beneficial bacteria such as *Lactobacillus* and *Bifidobacterium*, and to increases short-chain fatty acid production, which helps maintain intestinal homeostasis.[28,51] It is therefore plausible that COS-GL nanoparticles maintain favorable interactions with the intestinal microbiome, potentially contributing an additional layer of therapeutic benefit. Collectively, these findings suggest that the therapeutic efficacy of COS-GL nanoparticle is driven by the molecular integration of its components, enabling dual modulation of HMGB1 signaling and oxidative stress. The concurrent restoration of epithelial barrier integrity, sustained mucoadhesion, and prolonged colonic retention reflects a synergistic interplay between anti-inflammatory and barrier-stabilizing effects. COS-GL nanoparticle represents a "carrier-equals-drug" strategy that maximizes pharmacological content while minimizing formulation complexity. These mechanistic and structural advantages position COS-GL nanoparticle as a versatile and translationally promising nanomedicine for IBD.

Enhanced Mucoadhesive Properties and Stability of COS-GL Nanoparticles. For successful oral delivery, nanoparticles must remain stable during GI transit.[38,52,53] COS-GL nanoparticles maintained their structural integrity and surface charge in simulated intestinal conditions (pH 6) for over 12 h. While partial aggregation occurred in simulated gastric fluid (pH 2), the core structure remained sufficiently intact to ensure passage to the intestine (Figures 6A and S16). The mucoadhesive potential, critical for prolonging contact time, was confirmed using a turbidimetric assay, which showed strong binding between COS-GL nanoparticles and mucin (Figures 6B, S17 and S18). Ex vivo imaging of murine colonic tissue further confirmed that FITC-labeled COS-GL nanoparticles exhibited significantly higher retention in the colon at all time points compared to free FITC-labeled GL (Figures 6C,D and S19). This enhanced, targeted retention is paramount for improving therapeutic efficacy.

Crucially, during the 14 day repetitive oral administration in colitis model, we observed no evidence of mucus destruction or impaired nutrient absorption. Instead, the highest body weight gain was observed in the COS-GL-treated group (see Figure 5B), a significant indicator of overall health and effective nutrient utilization. Also, mucus regeneration was well preserved in colonic tissue (see Figure 5J). Furthermore, biochemical analysis showed normal levels of albumin and total protein in COS-GL-treated mice (see Figures S14 and S15), confirming the absence of systemic toxicity or malabsorption-related issues. These dynamic results suggests that the interaction of COS-GL nanoparticle is transient and does not induce long-term accumulation. Such a transient interaction is vital for ensuring the sustained function of the intestinal barrier. Moreover, chitosan-based mucoadhesive

https://doi.org/10.1021/acsnano.5c09985
ACS Nano XXXX, XXX, XXX−XXX

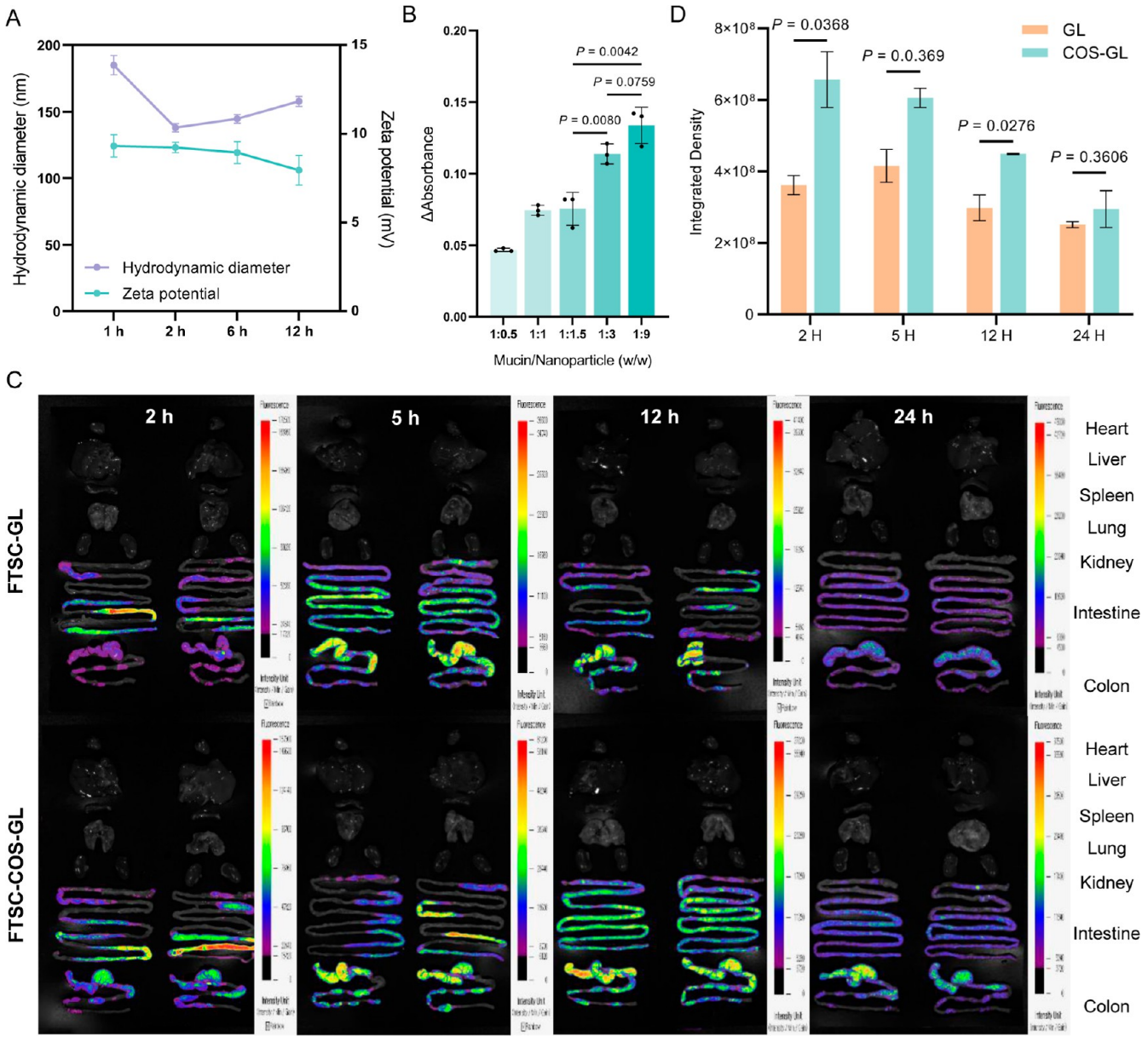

Figure 6. Enhanced mucoadhesive properties of COS-GL nanoparticles. (A) Hydrodynamic size changes and zeta potential changes of COS-GL nanoparticle exposed in pH 6 for 1, 2, 6, and 12 h. Data are expressed as mean ± SD (n = 3). (B) Turbidity of mucin. COS-GL nanoparticle mixtures as measured by UV absorbance at 500 nm. Data are expressed as mean ± SD (n = 3). (C,D) Fluorescence images (C) and histogram of fluorescence intensity (D) in colon of mice at 2, 5, 12, and 24 h after oral administration of FTSC-GL and FTSC−COS-GL (n = 2). For ex vivo fluorescence imaging, FTSC-labeled GL (40 mg·kg^{-1}), and FTSC-labeled COS-GL (50 mg·kg^{-1}) were administered with equivalent fluorescence labeling. Data are expressed as mean ± SD (n = 3). Statistical significance was determined by unpaired, two-tailed t-test in (B,D).

systems can extend gastrointestinal retention without negatively affecting cell-to-cell transport or nutrient absorption.[54,55] Collectively, the reversible mucosal adhesion and the absence of tissue abnormalities in this model indicate that COS-GL does not interfere with normal mucus regeneration or nutrient absorption, thereby supporting its potential for safe and prolonged therapeutic use.

CONCLUSIONS

In conclusion, this study reports the development and validation of orally administered COS-GL nanoparticles as a highly effective therapeutic platform for IBD. The rational design, based on conjugating the intrinsically antioxidative and mucoadhesive chitosan oligosaccharide (COS) with the anti-inflammatory drug glycyrrhizin (GL), yielded self-assembled nanoparticles with superior mucosal adhesion and prolonged retention at inflamed intestinal sites. These optimized physicochemical properties enabled targeted drug delivery while minimizing systemic exposure. Through comprehensive analyses using coculture systems, intestinal organoids, and a murine colitis model, we demonstrated that COS-GL nanoparticles exert a multimodal therapeutic effect. Mechanistically, they suppress ROS production, downregulate pro-inflammatory cytokine cascades, inhibit HMGB1-mediated signaling, and restore epithelial barrier integrity. Notably, the COS-GL nanoformulation consistently outperformed its individual

https://doi.org/10.1021/acsnano.5c09985
ACS Nano XXXX, XXX, XXX−XXX

components and the conventional IBD drug 5-ASA, underscoring a powerful therapeutic synergy. The ability of COS-GL to concurrently modulate the inflammatory microenvironment and actively promote mucosal healing addresses the multifactorial pathogenesis of IBD, a key limitation of many current therapies. Taken together, these findings establish COS-GL nanoparticles as a promising oral nanomedicine for IBD and provide a versatile platform for developing targeted therapies for other chronic inflammatory diseases

MATERIALS AND METHODS

Materials. Glycyrrhizin (GL), sodium periodate (SP), pyrene, lipopolysaccharide (LPS, from *E. coli* 0111:B4), Griess reagent, and mucin (from porcine stomach, type 3) were purchased from Sigma-Aldrich (St. Louis, MO, USA). Chitosan oligosaccharide (COS, <5 kDa) was obtained from Kittolife (Seoul, Korea). Dulbecco's Modified Eagle's Medium (DMEM), Fetal Bovine Serum (FBS), and penicillin−streptomycin were sourced from Welgene (Gyeongsan, Korea), CELLect, and Gibco (Grand Island, NY, USA), respectively. Dextran sodium sulfate (DSS, MW 36−50 kDa) was from TDB Consultancy (Uppsala, Sweden). All antibodies for immunofluorescence and flow cytometry were obtained from reputable commercial sources as detailed in the relevant sections. All other reagents were of analytical grade and used as received.

Synthesis and Self-Assembly of COS-GL Nanoparticles. Glycyrrhizin (GL, 50 mM in 10 mL carbonate buffer, pH 9.5, 4 °C) was oxidized by the dropwise addition of sodium periodate (SP, 50 mM in 10 mL deionized water (DW)). The reaction mixture was stirred sequentially in the dark (30 min) and under ambient light (30 min) to yield oxidized glycyrrhizin (oGL). A solution of chitosan oligosaccharide (COS, <5 kDa) in carbonate buffer was then added dropwise to the oGL solution and stirred at 4 °C for 24 h. To form a stable conjugate, the resulting imine bonds were reduced by adding 150 μL of 5 M sodium cyanoborohydride and stirring for an additional 24 h. Unreacted materials were removed by dialysis (MWCO: 3.5 kDa, VISKASE) against DW for 48 h. The purified COS-GL conjugate was obtained as a white powder via lyophilization (72 h). For experimental use, self-assembled COS-GL nanoparticles were prepared by sonicating a 1 mg·mL^{-1} aqueous solution at 37 °C for 10 min.

Characterization of COS-GL Nanoparticles. Fourier transform infrared (FT-IR) spectra were recorded on a Nicolet iS50 spectrometer (Thermo Fisher Scientific, Wilmington, DE, USA). ^{1}H NMR spectra were acquired in D_2O on a VNMRS 600 MHz spectrometer (Agilent Technologies, Santa Clara, CA, USA). Nanoparticle morphology and size were visualized using transmission electron microscopy (TEM; JEM 2100F, JEOL, Tokyo, Japan) on a carbon-coated copper grid. Hydrodynamic diameter, polydispersity index (PDI), and zeta potential were measured by dynamic light scattering (DLS) using a Zetasizer Nano ZS (Malvern Panalytical, Worcestershire, UK). The conjugation efficiency of GL was quantified using a NanoDrop 2000 UV−vis spectrophotometer (Thermo Fisher Scientific) by measuring absorbance at 259 nm. The critical micelle concentration (CMC) was determined using a pyrene fluorescence probe method. The ratio of emission intensities at 384 nm (I_3) and 373 nm (I_1) was plotted against the logarithm of the nanoparticle concentration.

Cell Culture. The murine macrophage cell line RAW 264.7 and the human colorectal adenocarcinoma cell line Caco-2 were obtained from the Korean Cell Line Bank (Seoul, Korea). Both cell lines were maintained in high-glucose DMEM supplemented with 10% FBS and 1% penicillin−streptomycin. Cells were cultured at 37 °C in a humidified atmosphere containing 5% CO_2

Cytotoxicity of COS-GL and In Vitro Dose Determination. Cell viability was assessed using the CCK-8 assay (Abbkine, Georgia, USA). Caco-2 cells and RAW 264.7 macrophages (1×10^4 cells/well) were seeded in a 96-well plate and cultured for 48 and 24 h, respectively. Cells were then treated with COS, GL, a physical mixture of COS/GL, or COS-GL nanoparticles at concentrations ranging from 0 to 2 mg·mL^{-1} for 24 h. Following treatment, cells were washed with PBS, and 10 μL of CCK-8 solution was added to each well with 100 μL of complete media. After a 2 h incubation in the dark, absorbance was measured at 450 nm using a microplate reader (BioTek Synergy H1, Winooski, VT, USA). No significant cytotoxicity was observed up to 1 mg·mL^{-1}, which was selected as the optimal concentration for subsequent experiments. Equivalent doses for COS (200 μg·mL^{-1}) and GL (800 μg·mL^{-1}) were determined based on the GL content within the nanoparticles.

ROS and RNA Scavenging by COS-GL Nanoparticle. For ROS scavenging, Caco-2 cells (1×10^4 cells/well) were seeded in a 96-well plate for 48 h. Cells were then cotreated with the respective drug formulations and H_2O_2 (100 μM) for 4 h. Intracellular ROS was quantified using 2 μM DCFH-DA (Thermo Fisher Scientific, Waltham, MA, USA) by measuring fluorescence at an excitation/emission of 490/520 nm. For RNS scavenging, RAW 264.7 cells (5×10^5 cells/well) were seeded in a 48-well plate, pretreated with the drug formulations for 5 h, and then stimulated with or without LPS (100 ng·mL^{-1}) for 20 h. Nitric oxide (NO) concentration in the supernatant was measured using Griess reagent by recording absorbance at 546 nm.

Tight Junction Recovery and Integrity. Caco-2 cells (2.6×10^5 cells/well) were cultured on 12-well polycarbonate filter inserts (0.4 μm pore size) for 4 weeks to form a differentiated monolayer. Transepithelial electrical resistance (TEER) was measured using a Millicell STX-2 voltmeter (Merck, Lisboa, Portugal). To assess recovery, monolayers were cotreated with drug formulations and H_2O_2 (100 μM) for 4 h. For immunofluorescence, cells were fixed with 4% paraformaldehyde (PFA), blocked with 20% goat serum, and incubated overnight at 4 °C with primary antibodies against ZO-1 (rabbit) and occludin (mouse) (1:100 dilution). Cells were then incubated with corresponding secondary antibodies (goat antirabbit-594 and goat antimouse-488, 1:200 dilution) and mounted with DAPI. To assess the role of calcium, H_2O_2-treated Caco-2 cells were loaded with Fluo-4 direct calcium reagent (invitrogen), and fluorescence was measured at an excitation/emission of 494/516 nm.

Intracellular Uptake of COS-GL Nanoparticles. COS-GL was fluorescently labeled with fluorescein-5-thiosemicarbazide (FTSC; Thermo Fisher Scientific) using EDC/NHS chemistry. For uptake studies, LPS-stimulated (100 ng·mL^{-1}, 20 h) and unstimulated RAW 264.7 macrophages were treated with 1 mg·mL^{-1} of FTSC−COS-GL for 1 h. Separately, Caco-2 cells were cotreated with FTSC−COS-GL and H_2O_2 (100 μM) for 4 h. After treatment, cells were fixed, stained with DAPI, and imaged using a fluorescence microscope.

Macrophage Polarization Analysis. RAW 264.7 cells (2×10^6 cells/well) were seeded in a 12-well plate, pretreated with drug formulations for 5 h, and stimulated with LPS (100 ng·mL^{-1}) for 20 h. Harvested cells were fixed, permeabilized, and stained with antibodies for M1 markers (CD80, iNOS) and M2 markers (CD206, CD163) (1:100 dilution). The ratio of M1/M2 polarized cells was analyzed by flow cytometry (BD FACSCalibur, BD Biosciences, San Jose, CA, USA).

Pro-Inflammatory Cytokines Analysis. RAW 264.7 cells (1.0×10^5 cells/well) were pretreated with drug formulations for 5 h and then stimulated with LPS (100 ng·mL^{-1}) for 20 h. For RT-PCR, total RNA was extracted (RNeasy Mini Kit, QIAGEN), reverse-transcribed to cDNA (iScript cDNA synthesis kit, Bio-Rad), and analyzed using SYBR Green PCR Master Mix (Applied Biosystems). Relative mRNA expression of TNF-α, IL-6, IL-1β, MCP-1, and iNOS was normalized to GAPDH. The primer sequences used are presented in Table S2. For ELISA, protein levels of TNF-α, IL-6, IL-1β, MCP-1, iNOS, and HMGB1 in the cell supernatant were quantified using commercially available kits per the manufacturer's instructions.

Caco-2/RAW 264.7 Coculture Model. Caco-2 cells (2×10^5 cells/well) were grown on Transwell inserts for 4 weeks. RAW 264.7 cells (3×10^5 cells/well) were seeded in the basal chamber. Drug formulations and H_2O_2 (100 μM) were added to the apical side (Caco-2) and incubated for 24 h. Cytokine expression in the basal

https://doi.org/10.1021/acsnano.5c09985
ACS Nano XXXX, XXX, XXX−XXX

RAW 264.7 cells and supernatant was analyzed by RT-PCR and ELISA.

Mucoadhesion Studies. For in vitro analysis, COS-GL solutions were mixed with a 2 mg·mL^{-1} mucin dispersion (pH 4.5). The interaction was quantified by measuring the change in turbidity (ΔAbs) of the mixture after 1 h of incubation. For ex vivo analysis, fluorescently labeled conjugates (FITC−COS-GL or FTSC−COS-GL) were orally administered to BALB/c mice. At 2, 5, 12, and 24 h postadministration, organs were excised, and nanoparticle retention was imaged using a fluorescence-labeled Organism Bioimaging Instrument (FOBI; CELLGENTEK Co., Cheongju-si, Korea).

Animals. Seven-week-old male BALB/c mice (Nara-Bio business, Seoul, Korea) and C57BL/6 mice (OrientBIO, Seongnam, Korea) were used in the in vivo investigations. All animals were housed in specific pathogen-free conditions and retained under the Institutional Animal Care and Use Committee (IACUC: 2023-0213) at Hanyang university.

Intestinal Organoid Culture. Intestinal crypts were isolated from mouse small intestine or colon by incubation in gentle cell dissociation reagent (STEMCELL Technologies). The isolated crypts were filtered, counted, and embedded in Matrigel Matrix (Corning). The domes were cultured in a 24-well plate with IntestiCult organoid growth medium (STEMCELL Technologies).

DSS-Induced Colitis Mouse Model. Seven-week-old male C57BL/6 mice were given 2.5% (w/v) DSS in drinking water for 7 days to induce colitis, followed by regular water for 7 days. Mice were orally administered daily with vehicle, COS (10 mg·kg^{-1}), GL (40 mg·kg^{-1}), 5-aminosalicylic acid (5-ASA, 50 mg·kg^{-1}), or COS-GL (50 mg·kg^{-1}). Body weight and stool status were monitored for 13 days.

Histological and Immunohistochemistry Analysis of Colon Tissue. Excised colon tissues were fixed in 4% PFA, embedded in paraffin, and sectioned (6 μm). For histological analysis, sections were stained with hematoxylin and eosin (H&E). For immunofluorescence, sections were deparaffinized and stained with primary antibodies against ZO-1, occludin, and MUC-2, followed by fluorescently labeled secondary antibodies and DAPI. Images were acquired with a fluorescence microscope.

Integrity of Tight Junction with Changes of Intracellular Calcium Concentration. Caco-2 cells (4×10^4 cells/well) were seeded in 96-well plate and incubated for 48 h. After washing with PBS, 200 μg·mL^{-1} of COS, 200 μg·mL^{-1} of GC, and 1 mg·mL^{-1} of COS-GL were reacted with H_2O_2 (100 μM), respectively, and added to each well to react for 4 h at 37 °C. After 4 h, add an equal volume of 2× Fluo-4 Direct calcium reagent loading solution (Fluo-4 Direct Calcium Assay Kits, Invitrogen) directly to wells containing cells in culture medium. Incubate plates at 37 °C for 30 min. Measure fluorescence using microplate reader for excitation at 494 nm and emission at 516 nm.

Statistical Analysis. All data are presented as mean ± standard deviation (SD). Statistical significance was determined using Student's *t*-test for two-group comparisons or one-way/two-way analysis of variance (ANOVA) for multiple-group comparisons using GraphPad Prism software. A *p*-value <0.05 was considered statistically significant.

ASSOCIATED CONTENT

Data Availability Statement

All relevant data are available with the article and its Supporting Information files or obtainable from the corresponding authors upon reasonable request.

Supporting Information

The Supporting Information is available free of charge at https://pubs.acs.org/doi/10.1021/acsnano.5c09985.

Detailed information on quantification of glycyrrhizin (GL) content in COS-GL nanoparticles; the primer sequences used in in vitro and in vivo experiment; cell viability of COS, GL, and COS-GL nanoparticles on RAW 264.7 macrophages and Caco-2 intestinal epithelial cells; cellular uptake of COS-GL nanoparticles in H_2O_2-stimulated Caco-2 cells; relative mRNA expression of pro-inflammatory cytokines in LPS-stimulated RAW 264.7 macrophages; histopathological analysis of major organs following 13 day consecutive treatment (PDF)

AUTHOR INFORMATION

Corresponding Author

Dong Yun Lee − *Department of Bioengineering, College of Engineering and Institute for Bioengineering and Biopharmaceutical Research (IBBR), and Institute of Nano Science and Technology (INST), Hanyang University, Seoul 04763, Republic of Korea; Elixir Pharmatech Inc., Seoul 04763, Republic of Korea;* orcid.org/0000-0001-7691-0447; Email: dongyunlee@hanyang.ac.kr

Authors

Gayoung Lim − *Department of Bioengineering, College of Engineering, Hanyang University, Seoul 04763, Republic of Korea*

Ha Rin Kim − *Division of Oncology, School of Medicine, Stanford University, Stanford, California 94305, United States; Biopharmaceutical Chemistry, Applied Chemistry, Kookmin University, Seoul 02707, Republic of Korea;* orcid.org/0000-0002-4342-1732

Chaerim Yoo − *Department of Bioengineering, College of Engineering, Hanyang University, Seoul 04763, Republic of Korea*

Yu Kyung Oh − *Department of Bioengineering, College of Engineering, Hanyang University, Seoul 04763, Republic of Korea*

Yeon Soo Park − *Department of Bioengineering, College of Engineering, Hanyang University, Seoul 04763, Republic of Korea*

Sijin Park − *Department of Bioengineering, College of Engineering, Hanyang University, Seoul 04763, Republic of Korea; Elixir Pharmatech Inc., Seoul 04763, Republic of Korea*

Seonmi Jang − *Department of Bioengineering, College of Engineering, Hanyang University, Seoul 04763, Republic of Korea*

Lia Priscilla − *Department of Bioengineering, College of Engineering, Hanyang University, Seoul 04763, Republic of Korea; Elixir Pharmatech Inc., Seoul 04763, Republic of Korea*

Complete contact information is available at: https://pubs.acs.org/10.1021/acsnano.5c09985

Author Contributions

#G.L., H.R.K., and C.Y contributed equally to this study. G.L., H.R.K., C.Y., Y.K.O, Y.S.P., and D.Y.L. conceived the research design. G.L., Y.K.O., Y.S.P., and S.P. performed the experiments. G.L., H.R.K., C.Y., Y.K.O., S.J., L.P., and D.Y.L. conducted data processing. G.L., H.R.K., and D.Y.L. contributed to analysis and interpretation of data. G.L., H.R.K., C.Y., Y.K.O., Y.S.P., and D.Y.L. grafted the manuscript. H.R.K., C.Y., and D.Y.L. edited the manuscript.

Notes

The authors declare the following competing financial interest(s): S.P., L.P. and D.Y.L. Lee reports a relationship with Elixir Pharmatech Inc. that includes: board membership

https://doi.org/10.1021/acsnano.5c09985
ACS Nano XXXX, XXX, XXX−XXX

and equity or stocks. The remaining other authors declare that they have no known competing financial interests or personal relationships that could have appeared to influence the work reported in this paper.

ACKNOWLEDGMENTS

This work was supported by the National Research Foundation (NRF) of Korea grant funded by the Ministry of MSIT (Project No. RS-2022-NR070744), the Korean Fund for Regenerative Medicine (KFRM) grant funded by the Korea government (the Ministry of Science and ICT, the Ministry of Health & Welfare) (Project No. KFRM24A0105L1, KFRM25A0107L1), and the Deeptech TIPS(TIPS) program funded by the Ministry of SMEs and Startups of Korea (Project No. RS-2023-00282845).

ABBREVIATIONS

IBD, inflammatory bowel disease; UC, ulcerative colitis; CD, Crohn's disease; GI, gastrointestinal; DAMPs, damage-associated molecular patterns; ROS, reactive oxygen species; RNS, reactive nitrogen species; 5-ASA, 5-aminosalicylic acid; HMGB1, high-mobility group box 1; IME, inflammatory microenvironment; RAGE, receptor for advanced glycation and endproducts; GL, glycyrrhizin; TLR4, toll-like receptor 4; GC, glycol chitosan; COS, chitosan oligosaccharide; COS-GL, chitosan oligosaccharide-glycyrrhizin; ABTS, 2,2-azino-bis-3-ethylbenzothiazoline-6-sulfonic acid; oGL, oxidized glycyrrhizin; TEM, transmission electron microscopy; CMC, critical micelle concentration; DCF-DA, 2′,7′-dichlorofluorescin diacetate; PBS, Phosphate-buffered saline; NO, nitric oxide; FITC, fluorescein isothiocyanate; CD, cluster of differentiation; TNF-α, tumor necrosis factor-α; IL-6, interleukin-6; IL-1β, interleukin-1β; MCP-1, monocyte chemoattractant protein-1; iNOS, inducible nitric oxide synthase; LPS, lipopolysaccharide; TEER, transepithelial electrical resistance; ZO-1, zonula occludens-1; OCLN, occludin; DSS, dextran sulfate sodium; DAI, disease activity index; RT-PCR, reverse transcription polymerase chain reaction; CALP, calprotectin; MUC, mucin

REFERENCES

(1) Kaplan, G. G. The global burden of IBD: from 2015 to 2025. *Nat. Rev. Gastroenterol Hepatol* **2015**, *12* (12), 720−727.
(2) Alatab, S.; Sepanlou, S. G.; Ikuta, K.; Vahedi, H.; Bisignano, C.; Safiri, S.; Sadeghi, A.; Nixon, M. R.; Abdoli, A.; Abolhassani, H.; et al. The global, regional, and national burden of inflammatory bowel disease in 195 countries and territories, 1990−2017: a systematic analysis for the Global Burden of Disease Study 2017. *Lancet Gastroenterol Hepatol* **2020**, *5* (1), 17−30.
(3) Zhao, M.; Gonczi, L.; Lakatos, P. L.; Burisch, J. The Burden of Inflammatory Bowel Disease in Europe in 2020. *J. Crohns Colitis* **2021**, *15* (9), 1573−1587.
(4) Boyapati, R. K.; Rossi, A. G.; Satsangi, J.; Ho, G. T. Gut mucosal DAMPs in IBD: from mechanisms to therapeutic implications. *Mucosal Immunol.* **2016**, *9* (3), 567−582.
(5) Muro, P.; Zhang, L.; Li, S.; Zhao, Z.; Jin, T.; Mao, F.; Mao, Z. The emerging role of oxidative stress in inflammatory bowel disease. *Front Endocrinol* **2024**, *15*, 1390351.
(6) Dunleavy, K. A.; Raffals, L. E.; Camilleri, M. Intestinal Barrier Dysfunction in Inflammatory Bowel Disease: Underpinning Pathogenesis and Therapeutics. *Dig. Dis. Sci.* **2023**, *68* (12), 4306−4320.
(7) Wang, X.; Peng, J.; Cai, P.; Xia, Y.; Yi, C.; Shang, A.; Akanyibah, F. A.; Mao, F. The emerging role of the gut microbiota and its application in inflammatory bowel disease. *Biomed Pharmacother* **2024**, *179*, 117302.
(8) Chelakkot, C.; Ghim, J.; Ryu, S. H. Mechanisms regulating intestinal barrier integrity and its pathological implications. *Exp. Mol. Med.* **2018**, *50* (8), 1−9.
(9) Martini, E.; Krug, S. M.; Siegmund, B.; Neurath, M. F.; Becker, C. Mend Your Fences: The Epithelial Barrier and its Relationship With Mucosal Immunity in Inflammatory Bowel Disease. *Cell Mol. Gastroenterol Hepatol* **2017**, *4* (1), 33−46.
(10) Cai, Z.; Wang, S.; Li, J. Treatment of Inflammatory Bowel Disease: A Comprehensive Review. *Front Med.* **2021**, *8*, 765474.
(11) Magro, F.; Cordeiro, G.; Dias, A. M.; Estevinho, M. M. Inflammatory Bowel Disease - Non-biological treatment. *Pharmacol. Res.* **2020**, *160*, 105075.
(12) Wang, K.; Zhu, Y.; Liu, K.; Zhu, H.; Ouyang, M. Adverse events of biologic or small molecule therapies in clinical trials for inflammatory bowel disease: A systematic review and meta-analysis. *Heliyon* **2024**, *10* (4), No. e25357.
(13) Hadji, H.; Bouchemal, K. Advances in the treatment of inflammatory bowel disease: Focus on polysaccharide nanoparticulate drug delivery systems. *Adv. Drug Deliv Rev.* **2022**, *181*, 114101.
(14) Kotla, N. G.; Singh, R.; Baby, B. V.; Rasala, S.; Rasool, J.; Hynes, S. O.; Martin, D.; Egan, L. J.; Vemula, P. K.; Jala, V. R.; et al. Inflammation-specific targeted carriers for local drug delivery to inflammatory bowel disease. *Biomaterials* **2022**, *281*, 121364.
(15) Mitragotri, S.; Burke, P. A.; Langer, R. Overcoming the challenges in administering biopharmaceuticals: formulation and delivery strategies. *Nat. Rev. Drug Discov* **2014**, *13* (9), 655−672.
(16) VanPatten, S.; Al-Abed, Y. High Mobility Group Box-1 (HMGb1): Current Wisdom and Advancement as a Potential Drug Target. *J. Med. Chem.* **2018**, *61* (12), 5093−5107.
(17) Chen, X.; Bao, S.; Liu, M.; Han, Z.; Tan, J.; Zhu, Q.; Huang, X.; Tian, X. Inhibition of HMGB1 improves experimental mice colitis by mediating NETs and macrophage polarization. *Cytokine* **2024**, *176*, 156537.
(18) Andersson, U.; Tracey, K. J. HMGB1 is a therapeutic target for sterile inflammation and infection. *Annu. Rev. Immunol.* **2011**, *29*, 139−162.
(19) Martinotti, S.; Patrone, M.; Ranzato, E. Emerging roles for HMGB1 protein in immunity, inflammation, and cancer. *Immunotargets Ther* **2015**, *4*, 101−109.
(20) Min, D. K.; Kim, Y. E.; Kim, M. K.; Choi, S. W.; Park, N.; Kim, J. Orally Administrated Inflamed Colon-Targeted Nanotherapeutics for Inflammatory Bowel Disease Treatment by Oxidative Stress Level Modulation in Colitis. *ACS Nano* **2023**, *17* (23), 24404−24416.
(21) Fan, H.; Tang, H. B.; Chen, Z.; Wang, H. Q.; Zhang, L.; Jiang, Y.; Li, T.; Yang, C. F.; Wang, X. Y.; Li, X.; et al. Inhibiting HMGB1-RAGE axis prevents pro-inflammatory macrophages/microglia polarization and affords neuroprotection after spinal cord injury. *J. Neuroinflammation* **2020**, *17* (1), 295.
(22) Oh, H.; Choi, A.; Seo, N.; Lim, J. S.; You, J. S.; Chung, Y. E. Protective effect of glycyrrhizin, a direct HMGB1 inhibitor, on post-contrast acute kidney injury. *Sci. Rep.* **2021**, *11* (1), 15625.
(23) Zhao, Z.; Xiao, Y.; Xu, L.; Liu, Y.; Jiang, G.; Wang, W.; Li, B.; Zhu, T.; Tan, Q.; Tang, L.; et al. Glycyrrhizic Acid Nanoparticles as Antiviral and Anti-inflammatory Agents for COVID-19 Treatment. *ACS Appl. Mater. Interfaces* **2021**, *13* (18), 20995−21006.
(24) Bakr, A. F.; Shao, P.; Farag, M. A. Recent advances in glycyrrhizin metabolism, health benefits, clinical effects and drug delivery systems for efficacy improvement; a comprehensive review. *Phytomedicine* **2022**, *99*, 153999.
(25) Shibata, N.; Ohno, T.; Shimokawa, T.; Hu, Z.; Yoshikawa, Y.; Koga, K.; Murakami, M.; Takada, K. Application of pressure-controlled colon delivery capsule to oral administration of glycyrrhizin in dogs. *J. Pharm. Pharmacol.* **2001**, *53* (4), 441−447.
(26) Kim, H. S.; Lee, S.; Lee, D. Y. Aurozyme: A Revolutionary Nanozyme in Colitis, Switching Peroxidase-Like to Catalase-Like Activity. *Small* **2023**, *19* (41), No. e2302331.
(27) Shen, C.; Zhao, L.; Du, X.; Tian, J.; Yuan, Y.; Jia, M.; He, Y.; Zeng, R.; Qiao, R.; Li, C. Smart Responsive Quercetin-Conjugated

https://doi.org/10.1021/acsnano.5c09985
ACS Nano XXXX, XXX, XXX−XXX

Glycol Chitosan Prodrug Micelles for Treatment of Inflammatory Bowel Diseases. *Mol. Pharmaceutics* **2021**, *18* (3), 1419−1430.
(28) Muanprasat, C.; Chatsudthipong, V. Chitosan oligosaccharide: Biological activities and potential therapeutic applications. *Pharmacol. Ther.* **2017**, *170*, 80−97.
(29) Rahman, A. T.; Shin, J.; Whang, C. H.; Jung, W.; Yoo, D.; Seo, C.; Cho, B. K.; Jon, S. Bilirubin Nanomedicine Rescues Intestinal Barrier Destruction and Restores Mucosal Immunity in Colitis. *ACS Nano* **2023**, *17* (11), 10996−11013.
(30) Mohyuddin, S. G.; Qamar, A.; Hu, C. Y.; Chen, S. W.; Wen, J. Y.; Liu, X. X.; Ma, X. B.; Yu, Z. C.; Yong, Y. H.; Wu, L. Y.; et al. Effect of chitosan on blood profile, inflammatory cytokines by activating TLR4/NF-κB signaling pathway in intestine of heat stressed mice. *Sci. Rep.* **2021**, *11* (1), 20608.
(31) Jing, B.; Xia, K.; Zhang, C.; Jiao, S.; Zhu, L.; Wei, J.; Wang, Z. A.; Chen, N.; Tu, P.; Li, J.; et al. Chitosan Oligosaccharides Regulate the Occurrence and Development of Enteritis in a Human Gut-On-a-Chip. *Front. Cell Dev. Biol.* **2022**, *10*, 877892.
(32) Chae, S. Y.; Jang, M. K.; Nah, J. W. Influence of molecular weight on oral absorption of water soluble chitosans. *J. Controlled Release* **2005**, *102* (2), 383−394.
(33) Chung, C. H.; Jung, W.; Keum, H.; Kim, T. W.; Jon, S. Nanoparticles Derived from the Natural Antioxidant Rosmarinic Acid Ameliorate Acute Inflammatory Bowel Disease. *ACS Nano* **2020**, *14* (6), 6887−6896.
(34) Kavi Rajan, R.; Hussein, M. Z.; Fakurazi, S.; Yusoff, K.; Masarudin, M. J. Increased ROS Scavenging and Antioxidant Efficiency of Chlorogenic Acid Compound Delivered via a Chitosan Nanoparticulate System for Efficient In Vitro Visualization and Accumulation in Human Renal Adenocarcinoma Cells. *Int. J. Mol. Sci.* **2019**, *20* (19), 4667.
(35) Aranaz, I.; Alcantara, A. R.; Civera, M. C.; Arias, C.; Elorza, B.; Heras Caballero, A.; Acosta, N. Chitosan: An Overview of Its Properties and Applications. *Polymers (Basel)* **2021**, *13* (19), 3256.
(36) Subramanian, D. A.; Langer, R.; Traverso, G. Mucus interaction to improve gastrointestinal retention and pharmacokinetics of orally administered nano-drug delivery systems. *J. Nanobiotechnology* **2022**, *20* (1), 362.
(37) Wang, Q. S.; Gao, L. N.; Zhu, X. N.; Zhang, Y.; Zhang, C. N.; Xu, D.; Cui, Y. L. Co-delivery of glycyrrhizin and doxorubicin by alginate nanogel particles attenuates the activation of macrophage and enhances the therapeutic efficacy for hepatocellular carcinoma. *Theranostics* **2019**, *9* (21), 6239−6255.
(38) Zhao, P.; Xia, X.; Xu, X.; Leung, K. K. C.; Rai, A.; Deng, Y.; Yang, B.; Lai, H.; Peng, X.; Shi, P.; et al. Nanoparticle-assembled bioadhesive coacervate coating with prolonged gastrointestinal retention for inflammatory bowel disease therapy. *Nat. Commun.* **2021**, *12* (1), 7162.
(39) Zhao, C.; Yang, J.; Chen, M.; Chen, W.; Yang, X.; Ye, H.; Wang, L.; Wang, Y.; Shi, J.; Yue, F.; et al. Synthetic Lignin-Derived Therapeutic Nano Reagent as Intestinal pH-Sensitive Drug Carriers Capable of Bypassing the Gastric Acid Environment for Colitis Treatment. *ACS Nano* **2023**, *17* (1), 811−824.
(40) Veider, F.; Sanchez Armengol, E.; Bernkop-Schnürch, A. Charge-Reversible Nanoparticles: Advanced Delivery Systems for Therapy and Diagnosis. *Small* **2024**, *20* (3), No. e2304713.
(41) Yoon, H. J.; Moon, M. E.; Park, H. S.; Im, S. Y.; Kim, Y. H. Chitosan oligosaccharide (COS) inhibits LPS-induced inflammatory effects in RAW 264.7 macrophage cells. *Biochem. Biophys. Res. Commun.* **2007**, *358* (3), 954−959.
(42) Weber, C. I. B. D. Lactococcus lactis alleviates oxidative stress and colitis in mice. *Nat. Rev. Gastroenterol Hepatol* **2015**, *12* (8), 429.
(43) Peng, J.; Li, H.; Olaolu, O. A.; Ibrahim, S.; Ibrahim, S.; Wang, S. Natural Products: A Dependable Source of Therapeutic Alternatives for Inflammatory Bowel Disease through Regulation of Tight Junctions. *Molecules* **2023**, *28* (17), 6293.
(44) Zhu, Y. X.; You, Y.; Chen, Z.; Xu, D.; Yue, W.; Ma, X.; Jiang, J.; Wu, W.; Lin, H.; Shi, J. Inorganic Nanosheet-Shielded Probiotics: A Self-Adaptable Oral Delivery System for Intestinal Disease Treatment. *Nano Lett.* **2023**, *23* (10), 4683−4692.
(45) Wirtz, S.; Neufert, C.; Weigmann, B.; Neurath, M. F. Chemically induced mouse models of intestinal inflammation. *Nat. Protoc.* **2007**, *2* (3), 541−546.
(46) Dieleman, L. A.; Palmen, M. J.; Akol, H.; Bloemena, E.; Peña, A. S.; Meuwissen, S. G.; Van Rees, E. P. Chronic experimental colitis induced by dextran sulphate sodium (DSS) is characterized by Th1 and Th2 cytokines. *Clin. Exp. Immunol.* **2001**, *114* (3), 385−391.
(47) Yokoe, J.; Iwasaki, N.; Haruta, S.; Kadono, K.; Ogawara, K.; Higaki, K.; Kimura, T. Analysis and prediction of absorption behavior of colon-targeted prodrug in rats by GI-transit-absorption model. *J. Controlled Release* **2003**, *86* (2−3), 305−313.
(48) Abinusawa, A.; Tenjarla, S. Release of 5-Aminosalicylic Acid (5-ASA) from Mesalamine Formulations at Various pH Levels. *Adv. Ther.* **2015**, *32* (5), 477−484.
(49) Mollica, L.; De Marchis, F.; Spitaleri, A.; Dallacosta, C.; Pennacchini, D.; Zamai, M.; Agresti, A.; Trisciuoglio, L.; Musco, G.; Bianchi, M. E. Glycyrrhizin binds to high-mobility group box 1 protein and inhibits its cytokine activities. *Chem. Biol.* **2007**, *14* (4), 431−441.
(50) Massier, L.; Bluher, M.; Kovacs, P.; Chakaroun, R. M. Impaired Intestinal Barrier and Tissue Bacteria: Pathomechanisms for Metabolic Diseases. *Front Endocrinol* **2021**, *12*, 616506.
(51) Wang, L.; Zhang, C.; Fan, S.; Wang, J.; Zhou, W.; Zhou, Z.; Liu, Y.; Wang, Q.; Liu, W.; Dai, X. Chitosan oligosaccharide improves intestinal homeostasis to achieve the protection for the epithelial barrier of female *Drosophila melanogaster* via regulating intestinal microflora. *Microbiol Spectr* **2024**, *12* (4), No. e03639.
(52) Date, A. A.; Hanes, J.; Ensign, L. M. Nanoparticles for oral delivery: Design, evaluation and state-of-the-art. *J. Controlled Release* **2016**, *240*, 504−526.
(53) Wang, Y.; Mo, Y.; Sun, Y.; Li, J.; An, Y.; Feng, N.; Liu, Y. Intestinal nanoparticle delivery and cellular response: a review of the bidirectional nanoparticle-cell interplay in mucosa based on physiochemical properties. *J. Nanobiotechnology* **2024**, *22* (1), 669.
(54) Kubbinga, M.; Nguyen, M. A.; Staubach, P.; Teerenstra, S.; Langguth, P. The Influence of Chitosan on the Oral Bioavailability of Acyclovir–a Comparative Bioavailability Study in Humans. *Pharm. Res.* **2015**, *32* (7), 2241−2249.
(55) Rosenthal, R.; Gunzel, D.; Finger, C.; Krug, S. M.; Richter, J. F.; Schulzke, J. D.; Fromm, M.; Amasheh, S. The effect of chitosan on transcellular and paracellular mechanisms in the intestinal epithelial barrier. *Biomaterials* **2012**, *33* (9), 2791−2800.

https://doi.org/10.1021/acsnano.5c09985
ACS Nano XXXX, XXX, XXX−XXX